CHAPTER 3

EXPERIMENTAL METHODS

3.1 Introduction

Three different systems were prepared i.e. MG30–single salt, MG30–double salt and MG30–salt–plasticizer systems. Characterization of the polymer electrolytes in this thesis will be carried out using the techniques discussed in this chapter.

Several techniques have been employed to identify the characteristics of the MG30 based polymer electrolyte. These techniques include x–ray diffraction (XRD), electrochemical impedance spectroscopy (EIS), scanning electron microscopy (SEM), and fourier transform infrared spectroscopy (FTIR). The film with the highest conductivity at room temperature will be further characterized using direct current polarization method.

3.2 Samples Preparation

All polymer electrolyte samples were prepared by the solvent or solution casting method. The MG30 polymer was supplied by Green HPSP Co., Malaysia and used as polymer host. Both lithium trifluoromethane sulfonate ($LiCF_3SO_3$) and lithium bis(trifluoromethane) sulfonamide ($LiN(CF_3SO_2)_2$) salts purchased from Aldrich were used as ion source. Both toluene and tetrahydrofuran (THF) procured from J.T. Baker were used as solvents. Poly(ethylene glycol) with relative molecular weight of 200

(PEG200) was obtained from Aldrich and used as plasticizer. All materials except for the salts were used without further purification.

3.2.1 Preparation of MG30–$LiCF_3SO_3$ system (Single–salt system)

$LiCF_3SO_3$ was dried for 2 hours at 130 ^oC to eliminate any trace amounts of water and MG30 was sliced into small pieces to ease the dissolution process. MG30 and $LiCF_3SO_3$ were dissolved in 40 mL toluene and 40 mL THF, respectively for 24 hours before being mixed together. The mixture was magnetically stirred for more than 72 hours at room temperature until both the polymer and salt were completely dissolved. The homogeneous solutions were then cast onto glass Petri dishes and allowed to dry to form films at room temperature. The films were kept in a desiccator with silica gel desiccants for further drying. The compositions of MG30 and $LiCF_3SO_3$ are shown in Table 3.1.

Table 3.1: Compositions of MG30–$LiCF_3SO_3$ system

Designation	MG30 (g)	$LiCF_3SO_3$ (g)	MG30 : $LiCF_3SO_3$ (wt. %)
MG0L	1.0	0.00	100:0
MG5L	1.0	0.05	95:5
MG10L	1.0	0.11	90:10
MG15L	1.0	0.18	85:15
MG20L	1.0	0.25	80:20
MG25L	1.0	0.33	75:25
MG30L	1.0	0.43	70:30
MG35L	1.0	0.54	65:35
MG40L	1.0	0.67	60:40

Table 3.1, continued

MG45L	1.0	0.82	55:45
MG50L	1.0	1.00	50:50

3.2.2 Preparation of MG30–$LiCF_3SO_3$–$LiN(CF_3SO_3)_2$ system (Double–salt system)

From MG30–$LiCF_3SO_3$ system, it was found that MG30 exhibited the highest ambient temperature conductivity at 30 wt. % $LiCF_3SO_3$. Based on this result, the double–salt polymer films were prepared using different ratios of $LiCF_3SO_3$ and $LiN(CF_3SO_2)_2$ with the total salt composition maintained at 30 wt. %.

Prior to use, both $LiCF_3SO_3$ and $LiN(CF_3SO_2)_2$ salts were heated in the oven for 2 hours at 130 ^oC to eliminate trace amounts of water. To prepare samples for the double–salt system, 1.0 g sliced MG30 was dissolved in toluene while the salts were stirred separately in THF for 24 hours at room temperature. The three homogeneous solutions were then mixed together and continuously stirred for over 72 hours. The solutions were then cast into different glass Petri dishes and left to dry to form films and then stored in a desiccator before further analyses. Table 3.2 summarizes the compositions of the prepared double–salt system.

Table 3.2: Compositions of MG30–$LiCF_3SO_3$–$LiN(CF_3SO_2)_2$ system

Designation	MG30 (g)	$LiCF_3SO_3$ (g)	$LiN(CF_3SO_3)_2$ (g)	MG30 : $LiCF_3SO_3$: $LiN(CF_3SO_2)_2$: PEG200 (wt. %)
MG20L10I	1.0	0.290	0.140	70 : 20 : 10 : 0
MG15L15I	1.0	0.215	0.215	70 : 15 : 15 : 0
MG10L20I	1.0	0.140	0.290	70 : 10 : 20 : 0

3.2.3 Preparation of MG30–$LiCF_3SO_3$–PEG200 system (Plasticized System)

This system was prepared in order to examine the influence of plasticizer content on the conductivity behavior of MG30–$LiCF_3SO_3$ system. The amount of $LiCF_3SO_3$ salt was fixed at 0.43 g which gives the highest ambient conductivity for MG30 single–salt system and varying amounts of PEG200 (5 to 30 wt. %) were prepared.

Pre–heated $LiCF_3SO_3$ salt and PEG200 were dissolved in THF while MG30 was dissolved in toluene for 24 hours. The polymer and salt–plasticizer solutions were then mixed together and were further stirred for 72 hours at room temperature. The homogeneous solutions were later cast onto glass Petri dishes and allowed to dry at room temperature to form films in the desiccator. The samples have been prepared as listed in Table 3.3.

Table 3.3: Compositions of MG30–$LiCF_3SO_3$–PEG200 system

Designation	MG30 (g)	$LiCF_3SO_3$ (g)	PEG200 (g)	MG30 : $LiCF_3SO_3$: PEG200 (wt. %)
MG30L–5P	1.0	0.43	0.075	66.5 : 28.5 : 5
MG30L–7P	1.0	0.43	0.11	65 : 28 : 7
MG30L–10P	1.0	0.43	0.16	63 : 27 : 10
MG30L–20P	1.0	0.43	0.36	56 : 24 : 20
MG30L–30P	1.0	0.43	0.61	49 : 21 : 30

3.3 X–ray Diffraction (XRD)

X–ray diffraction (XRD) is an important technique to obtain information up to atomic scale from both crystalline and amorphous materials. By observing the characteristic patterns of the X–ray diffractograms obtained, a material can be determined as crystalline or amorphous. The technique of XRD can be applied to indicate the occurrence of complexation between the polymer host and the doping salt. Complexation can be indicated by the shifts in peaks, changes in the relative intensities of peaks and existence or absence of peaks in the diffractograms of the samples [Sivakumar *et al.* 2006, Rajendra *et al.* 2004, Sreekanth *et al*, 1999, Reddy *et al*, 2007].

The diffraction intensity of films was measured using X–ray diffractometer (Siemens D5000) with operating voltage of 40 kV and current of 40 mA. The X–ray wavelength is 1.5406 Å. The X–rays impinge the films at 2 theta angles between 5° and 80°. The glancing angle increased in steps of 0.04°. As the sample rotates, the angles θ between the incident beam and the normal to the film is changed. X–rays hit the sample but some of the rays are diffracted. X–rays are reflected to the detector when the Bragg condition:

$$2d \sin\theta = n\lambda \qquad (3.1)$$

is satisfied. Here d is the interplanar spacing, θ is the Bragg angle, n is the order of diffraction and λ is the wavelength of X–ray. Example of XRD diffraction patterns of PMMA–grafted NR is shown in Figures 3.1 and 3.2.

Deconvolution of XRD peaks were carried out using OriginPro 8 software. A baseline was drawn from one end to another using autocreate method and was

subtracted from each XRD spectra. Multiple peaks were fitted manually using Gaussian function to separate overlapping XRD peaks.

According to Hodge *et al.* (1996), the crystalline fractions in samples can be predicted from the ratio of the integrated intensity of peaks associated with crystalline reflections to the integrated area of the spectrum by the equation below:

$$X_C = {A_C}/{A_T} \times 100 \qquad (3.2)$$

Where X_C is the crystalline fraction, A_T and A_C are the total and crystalline hump areas, respectively. Therefore, the degree of the crystalline factions can be estimated. Figure 3.1 shows the XRD patterns of MG49–based electrolytes incorporated with $LiBF_4$ salt and various types of fillers.

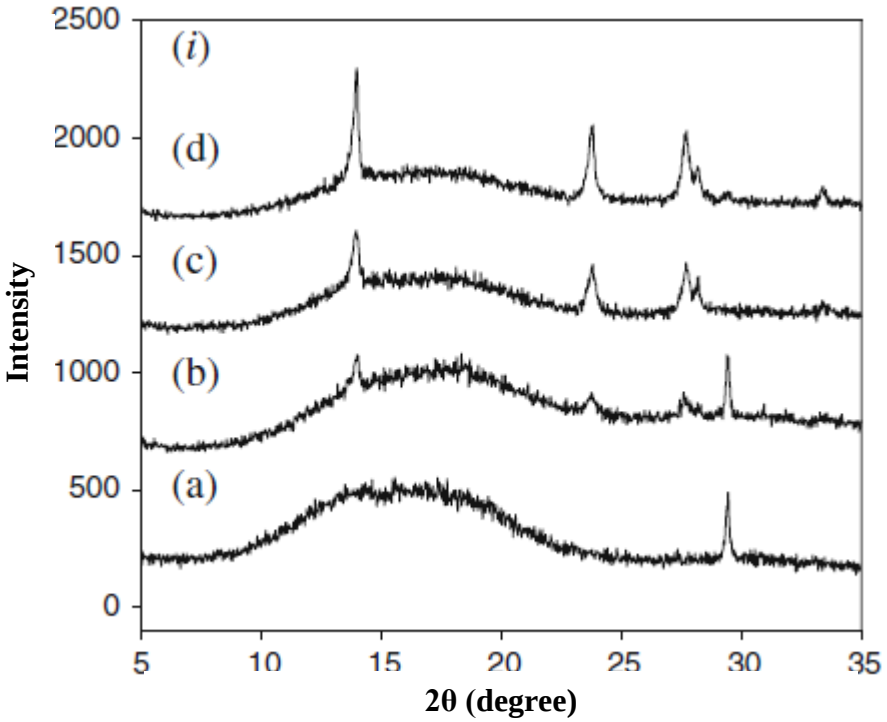

Figure 3.1 XRD diffractograms of (a) MG49–6 wt.% TiO_2, (b) MG49–30 wt.% $LiBF_4$–2 wt.% TiO_2, (c) MG49–30 wt.% $LiBF_4$–6 wt.% TiO_2 and (d) MG49–30 wt.% $LiBF_4$–10 wt.% TiO_2 [Low *et al.*, 2010b]

Referring to Low *et al.* (2010b), changes in the amorphousness of MG49 system have led to higher conductivity of the electrolytes due to higher mobility of charge carriers. Su'ait *et al.* (2009) confirmed that the increase of amorphous region of MG49 systems gives higher ionic conductivity as compared with the crystalline or semi–crystalline region because of the re–crystallization of $LiClO_4$ salt due to the ion association between Li^+ and CiO_4^- in the electrolyte at high salt concentration.

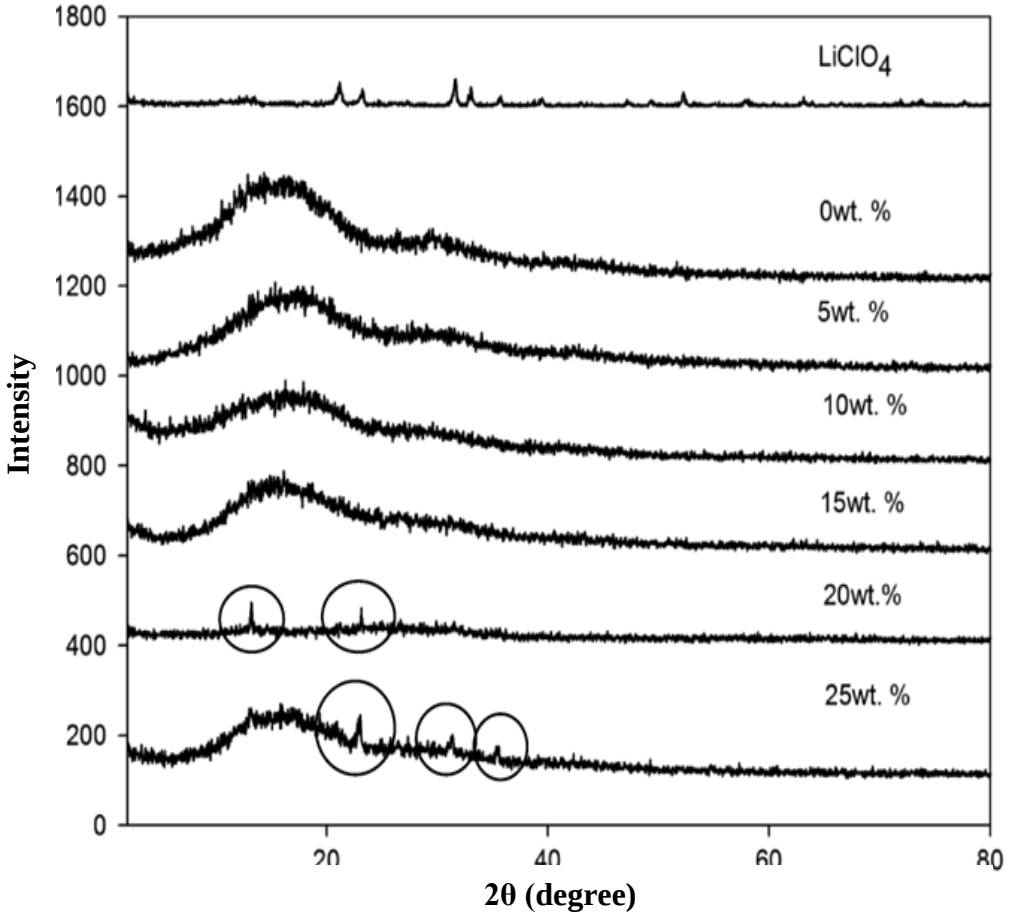

Figure 3.2 XRD diffractograms of 30/70 MG49–PMMA–$LiClO_4$ from 2^o to 80^o [Su'ait *et al.*, 2009]

3.4 Scanning Electron Microscopy (SEM)

The physical topology or morphology of the samples prepared can be observed using this technique. The uniformity of the blending and the salting effect of salt content and plasticizers on the morphology of the films can be determined.

Leica Stereoscan S440 model scanning electron microscope was used to capture the surface morphology images of the samples. Samples were coated with gold to prevent surface charging before the images were taken under vacuum. SEM micrographs can help to shed some important information to investigate the decrease and increase in conductivity. Examples of SEM micrographs are depicted in Figure 3.3.

Figure 3.3 shows the SEM micrographs for MG49–TiO_2–$LiClO_4$–*x*%EC reported by Low *et al.* (2010). It can be seen that the electrolyte surface is smoother with addition of EC. Therefore, Low *et al.* (2010) suggested that the MG49–TiO_2–$LiClO_4$–30 wt. % EC seems to be optimum for this system as Figure 3.3 (d) shows the smoothest surface morphology and thus facilitate the mobility of the ions in the polymer matrix.

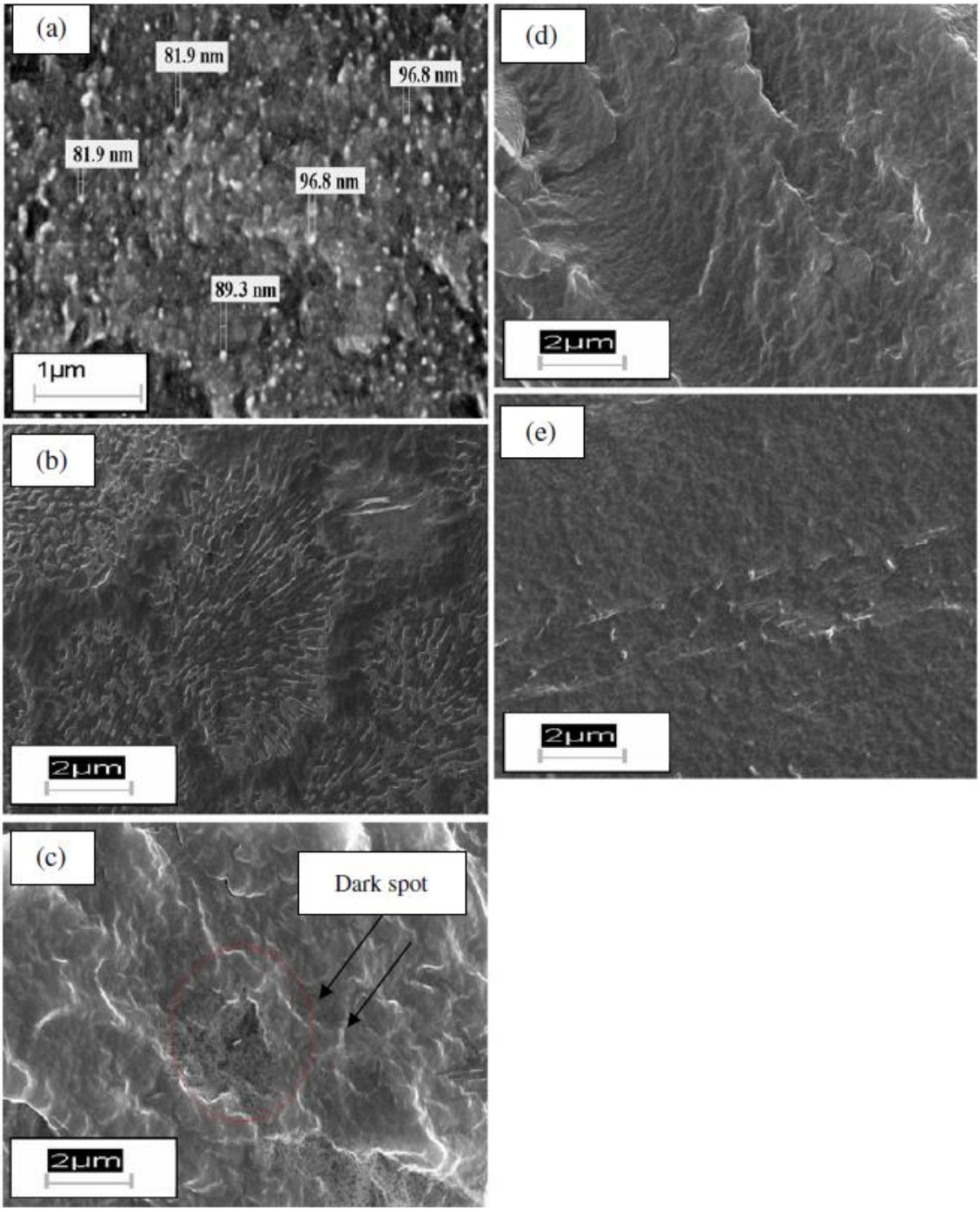

Figure 3.3 SEM micrographs of (a) MG49–TiO_2–$LiClO_4$, (b) 0 wt. % EC, (c) 10 wt. % EC, (d) 30 wt. % EC and (e) 50 wt. % EC [Low *et al.*, 2010b]

3.5 Fourier Transform Infrared Spectroscopy (FTIR)

The interactions between the polymer hosts, salt(s) and plasticizer can be determined by FTIR studies. FTIR has been employed by many researchers [Majid and Arof (2005); Kumutha and Alias (2006); Ramesh and Chai (2007)] to determine the occurrence of complexation between polymer and salt. In this work, IR spectra were recorded using the Thermo Scientific/Nicolet iS10 spectrophotometer at room temperature in the wavenumber region from 4000 cm^{-1} to 650 cm^{-1} to verify the occurrence of complexation between MG30, $LiCF_3SO_3$, $LiN(CF_3SO_2)_2$ and PEG200. The resolution used was 1 cm^{-1}. Figure 3.4 shows the FTIR spectrum of pure MG30 sample. The vibrational modes of MG30 are listed on Table 3.4.

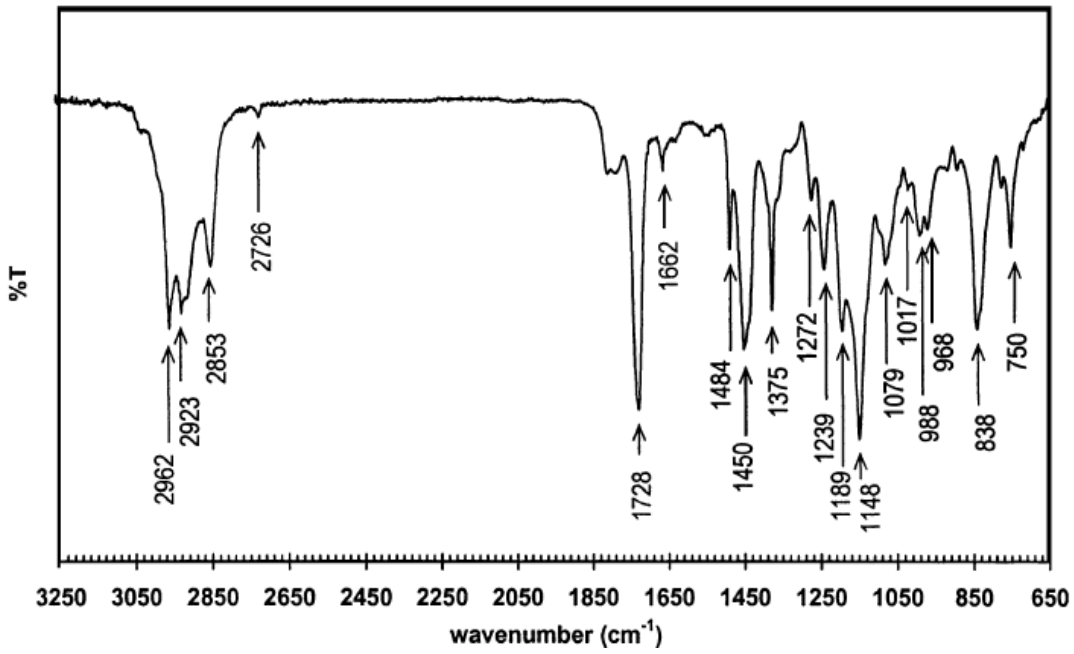

Figure 3.4 FTIR spectra in the wavenumber range from 3250 to 650 cm^{-1} of pure MG30 [Ali *et al.*, 2008]

Table 3.4: FTIR vibrational bands of PMMA–grafted natural rubber (i.e. MG30 and MG49) obtained from literature

Assignment	Wavenumber (cm^{-1})	Reference
$v_{as}(CH_3)$ of PMMA	2962	Ali *et al.*, 2008
	2960	Alias *et al.*, 2005
$v_{as}(CH_2)$ of PMMA	2923	Ali *et al.*, 2008
$v_s(CH_2)$ of PMMA	2853	Ali *et al.*, 2008
C–H stretch	2726	Ali *et al.*, 2008
v(C=O) of PMMA	1729	Ali *et al.*, 2006,
	1728	Ali *et al.*, 2008
	1724	Alias *et al.*, 2005
v(C=C) of polyisoprene	1662	Ali *et al.*, 2008
$v_{as}(CH_3)$ of PMMA	1484	Ali *et al.*, 2008
O–CH_3 asymmetric deformation of PMMA	1450	Ali *et al.*, 2008
	1447	Kumutha *et al.*, 2005
Bending of CH_3 group of PMMA	1445	Ali *et al.*, 2006
$\delta(OCH_3)$ of PMMA	1390	Alias *et al.*, 2005
O–CH_3 deformation of PMMA	1387	Kumutha *et al.*, 2005
Bending of CH_3 group of PMMA	1375	Ali *et al.*, 2006, Ali *et al.*, 2008
v(C–O) of –COO– of PMMA	1274	Kumutha *et al.*, 2005
	1272	Ali *et al.*, 2008
CH_2 twisting	1239	Ali *et al.*, 2008
C–H_2 in plane bending of polyisoprene	1189	Ali *et al.*, 2008
CH_2 twisting of PMMA	1148	Ali *et al.*, 2008
CH_3 rocking of polyisoprene	1079	Ali *et al.*, 2008
v(C–C) of polyisoprene	1017	Ali *et al.*, 2008
v_s(C–O–C) of PMMA	988	Ali *et al.*, 2008
	987	Kumutha *et al.*, 2005
	984	Alias *et al.*, 2005

Table 3.4, continued

$C–H_2$ out of plane bending of polyisoprene	968	Ali *et al.*, 2008
$C(CH_3)_2$ skeletal vibration of PMMA	838	Ali *et al.*, 2008
CH_2 rocking of PMMA	750	Ali *et al.*, 2008

The FTIR spectra of MG30–based polymer electrolytes are shown in Figure 3.5.

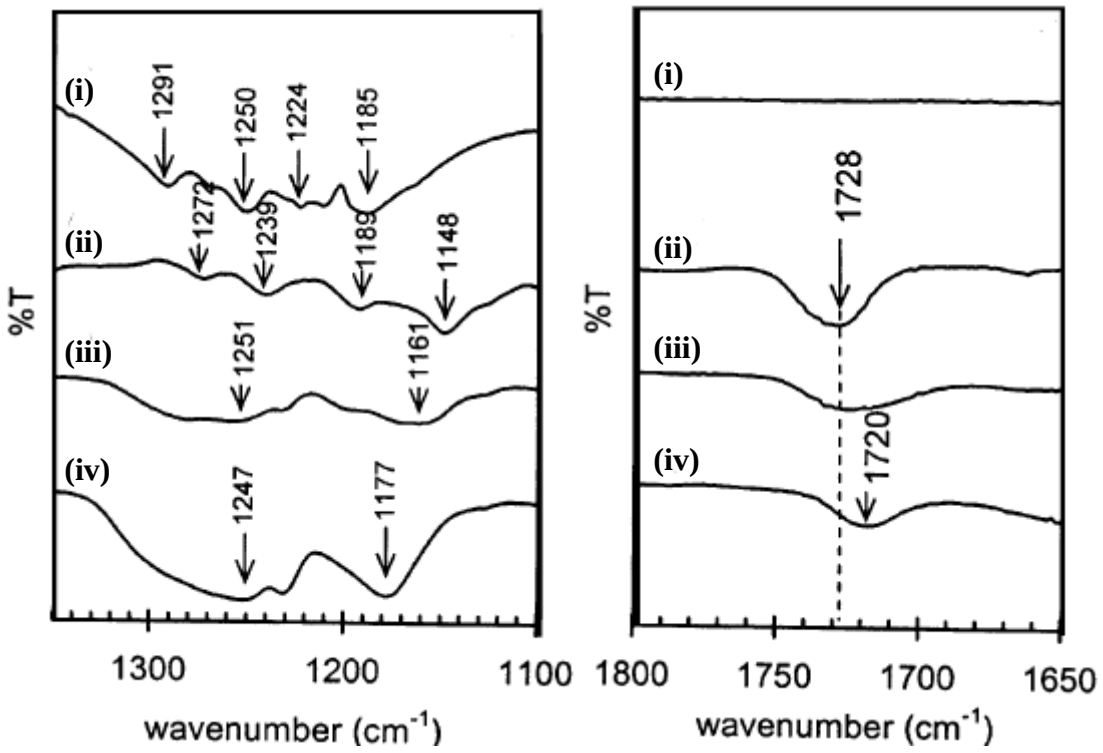

Figure 3.5 FTIR spectra in the wavenumber range between (a) 1350 to 1100 cm^{-1} and (b) 1650 to 1800 cm^{-1} for (i) pure $LiCF_3SO_3$, (ii) pure MG30, (iii) MG30–35 wt. % $LiCF_3SO_3$ and (iv) MG30–45 wt. % $LiCF_3SO_3$. [Ali *et al.*, 2008]

The most intense, very strong and sharp peak for the carbonyl functional group (C=O) from PMMA, which was grafted to the main chain of NR is always being chosen as an indicator for detecting the occurrence of complexation between polymer and metal ion. It is represented by the band that peaks between 1723 to 1731 cm^{-1} [Kumutha *et al.*, 2004; Ali *et al.*, 2008]. Polymer–salt complex is formed when lithium salts are dissolved in the polymer matrix. The Li^+ cations can form a dative bond with the

oxygen atom in the carbonyl group resulting in the downshift of the carbonyl band from 1731 cm^{-1} to in between 1724 cm^{-1} [Deepa *et al.*, 2002; Deepa *et al.*, 2004]. These observations imply the occurrence of complexation between the incorporated salt and the oxygen atom of the C=O groups of MG30. Besides that, a shift in the O–CH_3 band from 1390 cm^{-1} to 1387 cm^{-1} and a shift in the –COO– band from 1272 cm^{-1} to 1274 cm^{-1} [Alias *et al.*, 2005 and Ali *et al.*, 2008] also do indicate that interaction takes place between metal ion with oxygen atom which bear a lone pair electron.

Deconvolution of selected IR regions was performed using OMNIC software. The deconvolution was carried out by fixing the number and line shape, and allowing band parameters such as full width at half maximum (FWHM), area, intensity and band shape to vary without constraints during the iteration [Brooksby and Fawcett, (2000)]. The Gaussian/Lorentzian function was employed to fit the selected bands.

3.6 Electrochemical Impedance Spectroscopy (EIS)

Impedance measurements of the films were carried out using the HIOKI 3531–01 LCR Hi–tester that was interfaced to a computer. The impedance was measured in the frequency range from 50 Hz to 1 MHz in the temperature range from 298 K to 393 K. All samples were sandwiched between two stainless steel electrodes with a diameter of 1 cm under spring pressure. The conductivity of the films can be calculated using the following equation:

$$\sigma = \frac{t}{R_b A} \qquad (3.3)$$

where σ is the conductivity of the sample, t is the thickness of sample, A is the area of contact between sample film and electrode, and R_b is the bulk impedance of sample obtained from the Cole–Cole plot of negative imaginary impedance versus real

impedance. The impedance for each sample was measured six times for each sample prepared.

Other functions in impedance spectroscopy are complex admittance *A* (w), complex permittivity ε (w) and complex electrical modulus *M* (w) which can be derived from the impedance data. The relationship between admittance and impedance is given by:

$$A(w) = \frac{Z'}{(Z'^2 + Z''^2)} - \frac{jZ''}{(Z'^2 + Z''^2)} \tag{3.4}$$

The relationship between complex permittivity and impedance is given by:

$$\varepsilon(w) = \frac{Z''}{\omega C_o (Z'^2 + Z''^2)} + \frac{jZ'}{\omega C_o (Z'^2 + Z''^2)} \tag{3.5}$$

The relationship between modulus and complex permittivity is given by:

$$M(w) = \frac{\varepsilon'}{(\varepsilon'^2 + \varepsilon''^2)} - \frac{j\varepsilon''}{(\varepsilon'^2 + \varepsilon''^2)} \tag{3.6}$$

The loss tangent equation can be written as,

$$\tan \partial = \frac{M''}{M'} \tag{3.7}$$

or

$$\tan \partial = \frac{\varepsilon''}{\varepsilon'} \tag{3.8}$$

The terms in equation stated above is defined as follows:

w = $2\pi f$ (angular frequency)

C_o = Vacuum capacitance of the empty cell

Z' = $Z\cos\theta$

Z'' = $Z\sin\theta$

j = $\sqrt{-1}$

Alias *et al.* (2005) and Ali *et al.* (2006) have studied the conductivity of natural rubber (NR) grafted with poly(methyl methacrylate) (PMMA) system separately. Through the impedance analysis (Figure 3.6 and Figure 3.7), they both found that the conductivity for MG polymer electrolyte is thermally assisted and interestingly both their samples exhibit Arrhenius conductivity–temperature relationship in the temperature range between 298 K to 333 K. Figure 3.8 and Figure 3.9 (Ali *et al.*, 2006) show that Cole–Cole plot of the MG30 may consist of only a tilted spike or semicircle followed by a spike tail even in the highly plasticizer condition.

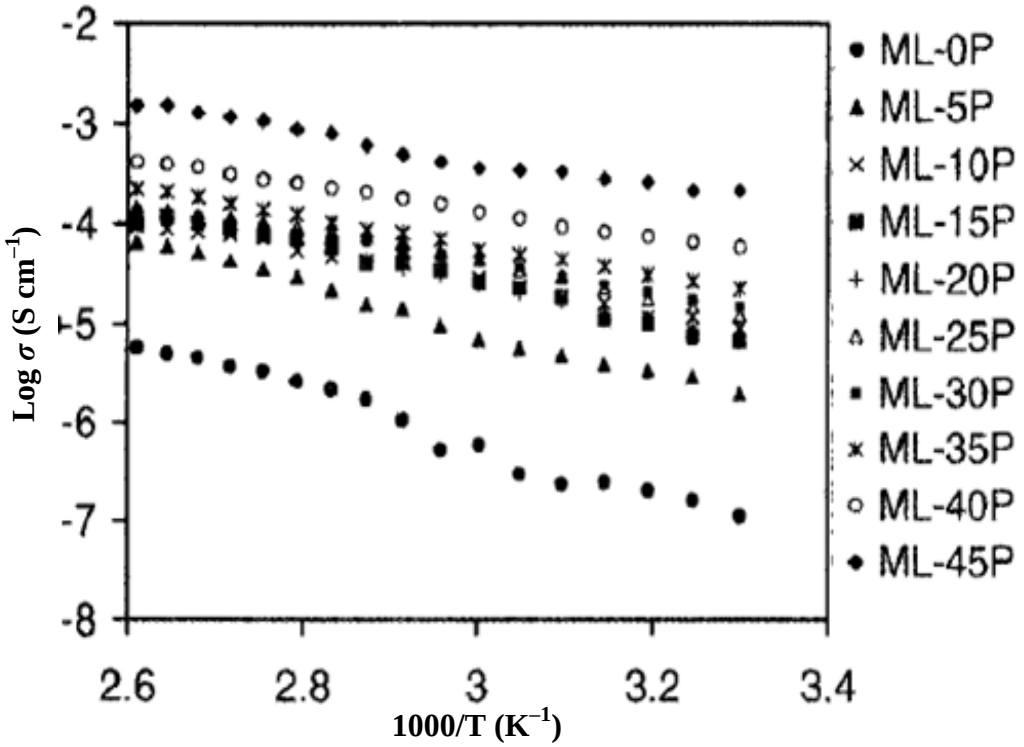

Figure 3.6 Arrhenius plots of MG49 polymer electrolyte system as a function of PC wt. % at different temperatures [Alias *et al.*, 2005]

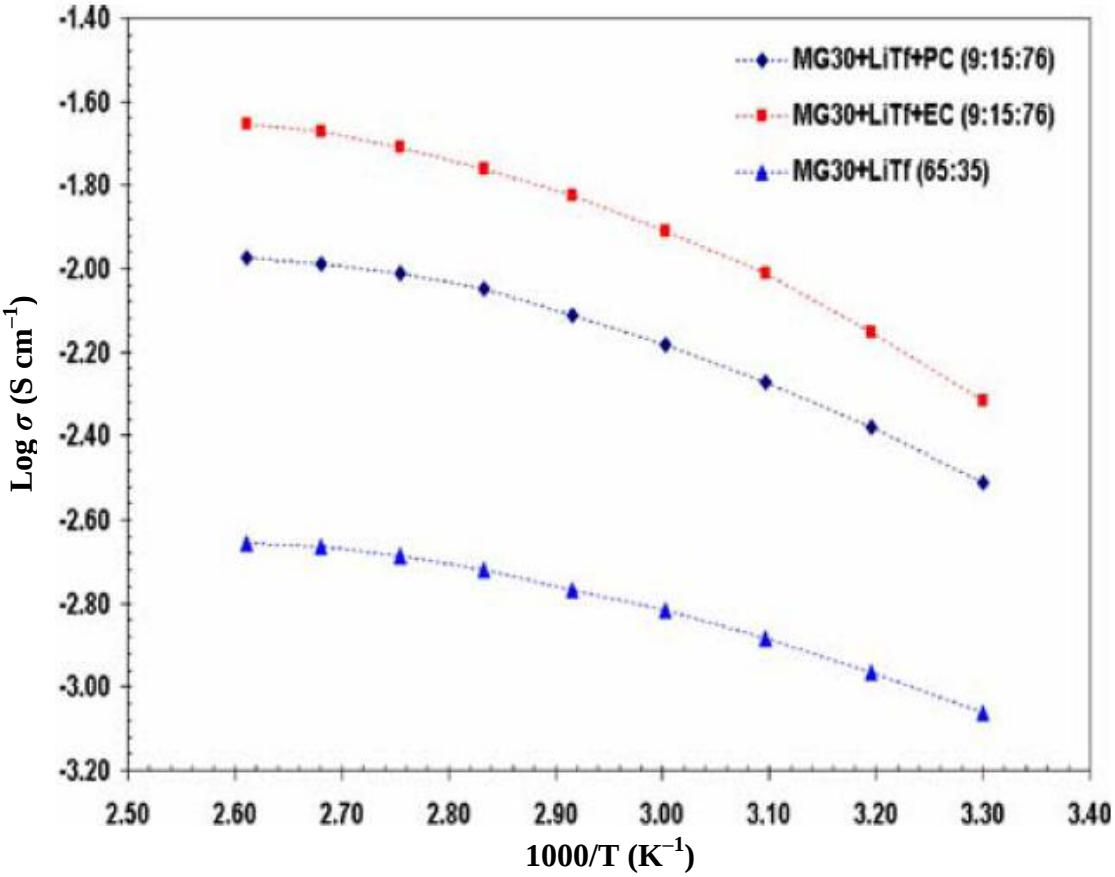

Figure 3.7 Temperature–dependent conductivity plots of the plasticized and unplasticized GPEs [Ali *et al.*, 2006]

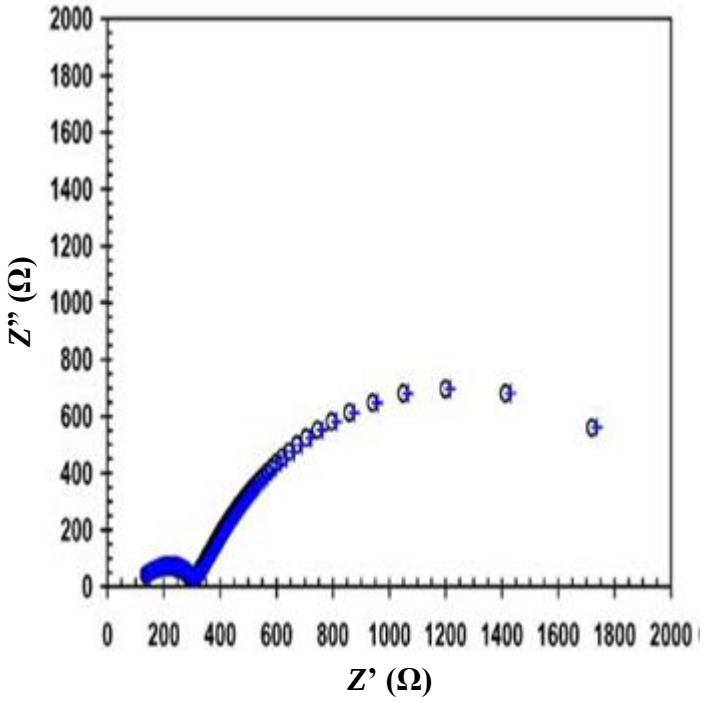

Figure 3.8: Cole–Cole plot of MG30–$LiCF_3SO_3$–EC (9:15:76) sample [Ali *et al.*, 2006]

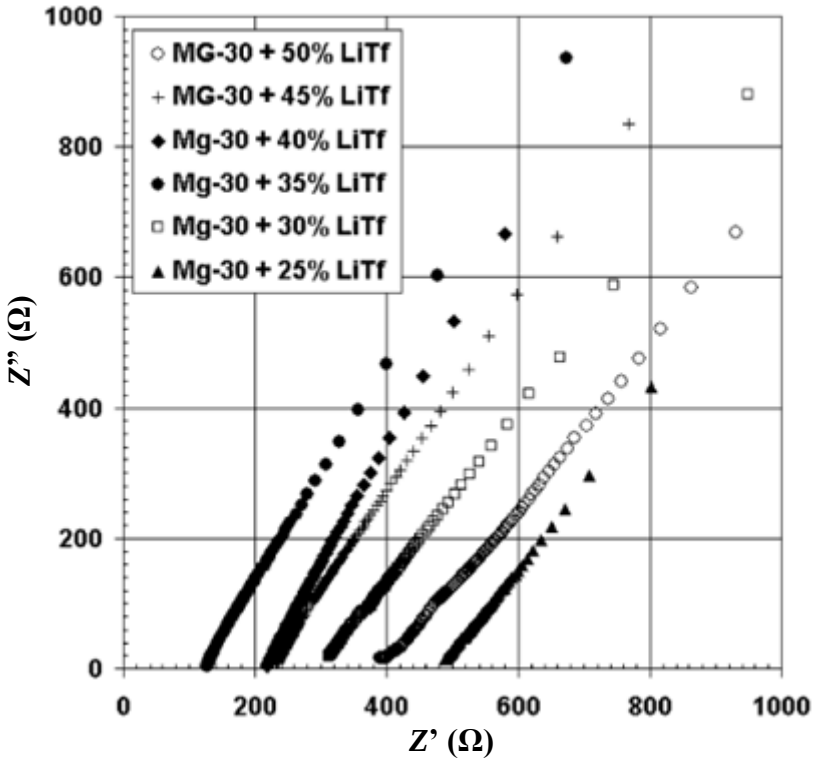

Figure 3.9 Cole–Cole plots of GPEs containing various amounts of $LiCF_3SO_3$ [Ali *et al.*, 2006]

3.7 Transference number measurements by Wagner's Polarization Method

The electrolyte films prepared are supposed to be ionic conductor. The transference number can be used to indicate the conducting species in an electrolyte. The transference number of an electrolyte can be measured by direct current polarization method. If the conductivity of the samples is primarily contributed by ions, the current flows through the electrode will fall rapidly with time, whereas on the other hand the current of a non ion–conductor sample would not decrease with time.

The experiments are made up of two steps and the samples will be sandwiched between:

(1) Two stainless steel (SS) blocking electrodes in the SS/Electrolyte/SS configuration. Therefore the transference number of electron (T_e) and ionic (T_i) can be calculated as follow:

$$T_e = I_S / I_0 \tag{3.9}$$

$$T_i = (I_0 - I_S) / I_0 \tag{3.10}$$

(2) Two non–blocking lithium electrodes in the Li/Electrolyte/Li symmetrical configuration. The transference number of cationic (T_+) and anionic (T_-) can be calculated as follow:

$$T_{i+e} = I_S / I_0 \tag{3.11}$$

$$T_+ = T_{i+e} - T_e \tag{3.12}$$

Figure 3.10 shows that by using transference number, Ali *et al.* (2006) have confirmed that the ionic conductivity of MG30 mainly depends on anion transport with a low lithium ions transference number of 0.23.

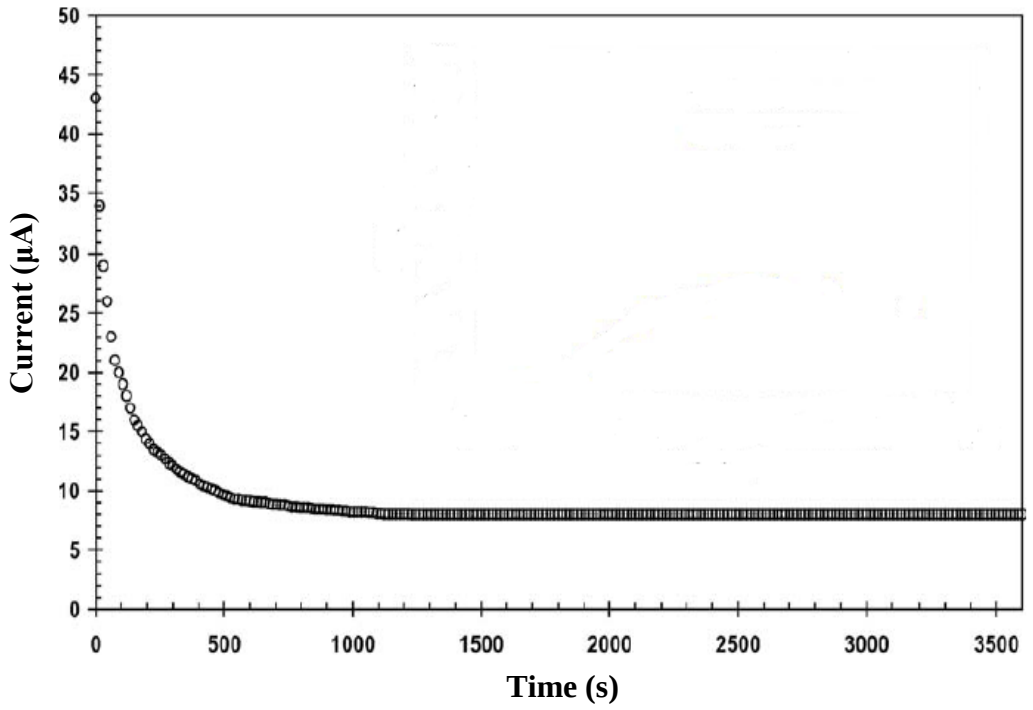

Figure 3.10 The chronoamperometry of MG30–$LiCF_3SO_3$–EC (9:15:76) under constant voltage of 10 mV [Ali *et al.*, 2006]

3.8 Summary

Results and discussion which conducted using the above mentioned methods will be discussed in the following chapter.